Published in final edited form as:
Dev Cell. 2014 August 25; 30(4): 449–462. doi:10.1016/j.devcel.2014.06.012.

Parasympathetic innervation regulates tubulogenesis in the developing salivary gland

Pavel I. Nedvetsky[2,‡,6], **Elaine Emmerson**[1,6], **Jennifer Finley**[1], **Andreas Ettinger**[1], **Noel Cruz-Pacheco**[1], **Jan Prochazka**[3], **Candace L. Haddox**[4], **Emily Northrup**[1], **Craig Hodges**[5], **Keith E. Mostov**[2], **Matthew P. Hoffman**[4], and **Sarah M. Knox**[1,*]

[1]Department of Cell & Tissue Biology, University of California San Francisco, San Francisco CA 94143 USA

[2]Department of, Anatomy, University of California San Francisco, San Francisco CA 94143 USA

[3]Department of, Orofacial Sciences, University of California San Francisco, San Francisco CA 94143 USA

[4]National Institute of Dental and Craniofacial Research, Bethesda MD 20892 USA

[5]Department of Genetics and Genome Sciences, Case Western Reserve University, Cleveland, OH 44106 USA

Abstract

A fundamental question in development is how cells assemble to form a tubular network during organ formation. In glandular organs tubulogenesis is a multistep process requiring coordinated proliferation, polarization and reorganization of epithelial cells to from a lumen, and lumen expansion. Although it is clear that epithelial cells possess an intrinsic ability to organize into polarized structures, the mechanisms coordinating morphogenetic processes during tubulogenesis are poorly understood. Here, we demonstrate that parasympathetic nerves regulate ductal tubulogenesis in the developing salivary gland. We show that the neurotransmitter vasoactive intestinal peptide (VIP) secreted by the innervating ganglia promotes ductal growth, leads to the formation of a contiguous lumen, and facilitates lumen expansion through a cAMP/PKA-dependent pathway. Furthermore, we provide evidence that lumen expansion is independent of apoptosis and involves the cystic fibrosis transmembrane conductance regulator (CFTR), a cAMP-regulated Cl(−) channel. Thus, parasympathetic innervation coordinates multiple steps in tubulogenesis during organ formation.

*Corresponding author: sarah.knox@ucsf.edu, Phone: + 1 (415) 502-0811.
‡present address: Vascular Patterning Laboratory, Vesalius Research Center, VIB and KU Leuven, B-3000 Leuven, Belgium
6co-first author

Author Contributions: P.N. performed and analyzed most of the cAMP/PKA experiments. E.E. performed and analyzed most of the ex vivo VIPR1ant culture experiments. Both P.N and E.E. participated in the writing of the manuscript.

Introduction

Tubulogenesis during glandular development results in the establishment of a complex network of epithelial ducts with terminal acini (Lubarsky and Krasnow, 2003). While subcellular mechanisms govern polarization of individual and neighboring epithelial cells, formation of a complex tubular network *in vivo* largely relies on interactions with the stroma, which consists of endothelial, mesenchymal and neuronal cells, as well as the extracellular matrix (rev. by (Iruela-Arispe and Beitel, 2013)). Despite the progress made towards our understanding of tubulogenesis, the mechanisms controlling coordinated behavior of epithelial cells to form a functional tube remains poorly understood.

A potential mechanism to coordinate epithelial tubulogenesis involves the parasympathetic branch of the autonomic nervous system, which innervates all tubular organs including the lungs, prostate and salivary glands. The developing submandibular gland (SMG; embryonic day (E) 11.5 to 15) is innervated by the parasympathetic, but not sympathetic or sensory, nerves of the parasympathetic submandibular ganglion (PSG) (Proctor and Carpenter, 2007). Ductal tubulogenesis is also occurring in parallel with PS innervation. We recently showed that the PSG maintains a reservoir of undifferentiated keratin (K) 5 (+) progenitor cells via an acetylcholine (ACh)/muscarinic (M1) receptor/epidermal growth factor receptor (EGFR)-dependent pathway in the *ex vivo* embryonic SMG (Knox et al., 2010). Signals from the PSG also control the function of adult SMG and also maintain epithelial architecture, as tissue degeneration results from parasympathetic denervation of rodent or human salivary gland epithelium (Kang et al., 2010; Kyriacou and Garrett, 1988; Mandour et al., 1977). However, it is unclear whether the role of innervation is exclusively to drive progenitor cell proliferation, thereby ensuring a sufficient supply of epithelial cells, or if this role extends to direct regulation of epithelial tubulogenesis (e.g. cell polarization, duct and lumen formation).

Here, we show that parasympathetic nerves play a multifunctional role in tubulogenesis during SMG organogenesis. Ductal tubulogenesis in the SMG requires differentiated luminal cells (K19(+)) to proliferate and then condense at the midline, which occurs at E13.5. These cells polarize to form microlumens that coalesce to form a contiguous ductal lumen (Hieda et al., 1996) (~E14; Figure 1A and Figure S1). Finally the lumen expands for the passage of liquids (Figure 1A). During this process, axon bundles migrate from the PSG along the basement membrane surrounding the ductal epithelium to envelope the end buds (Coughlin, 1975; Knox et al., 2010). Nerve-derived factors released from varicosities (non-conventional synapses) on the axons diffuse towards the epithelium, thus establishing neuronal-epithelial communication. Here we identify neuronal-derived vasoactive intestinal peptide (VIP) as an important regulator of key steps during epithelial tubulogenesis. VIP activates the cAMP/PKA pathway to increase duct elongation through cell proliferation and the subsequent formation of a single contiguous lumen through fusion of multiple microlumens. Once the lumen has formed, VIP is also required for its expansion via a cAMP/PKA/CFTR-dependent pathway.

Results

Ductal tubulogenesis is aberrant in the absence of parasympathetic innervation

Based on the parallel development of nerves and epithelium, we postulated that neuronal signals modulate ductal tubulogenesis. To test this hypothesis, we inhibited neuronal outgrowth and function in E13 SMG *ex vivo* cultures using a function-blocking antibody to the neurotrophic factor neurturin (NRTN). NRTN is secreted by the end buds and binds its cognate receptor GFRα2 on the nerves to promote neuronal outgrowth, function and survival (Knox et al., 2013). Similar to our prior study, inhibition of NRTN signaling resulted in reduced nerve outgrowth and deficient innervation of the epithelium as well as decreased epithelial branching (Figure 1B; (Knox et al., 2013). To examine ductal tubulogenesis we used the tight junction marker protein zona occludin-1 (ZO1). ZO1(+) tight junctions form at the border between basolateral and apical (luminal) membranes and thus can be used to highlight sites of ductal lumen formation (Figure S1). In control SMG, ZO1 immunostaining revealed an interconnected network of tight junctions demarcating the developing ductal lumen (Figure 1D, control IgG). However, in anti-NRTN treated SMG, ZO1(+) structures were distributed throughout the epithelium, with little to no localization at the ductal midline or interconnections between individual structures (Figure 1D, lower panel). Thus, loss of NRTN/GFRα2 signaling and consequently innervation disrupts lumen formation during SMG development.

VIP/VIPR1 but not ACh/M1 signaling is required for ductal tubulogenesis

Given that neuronal ACh increases SMG growth by activating epithelial muscarinic receptors (Knox et al., 2010), we asked whether muscarinic signaling also regulates ductal tubulogenesis. Culture of intact E12.5 SMG with the muscarinic antagonist 4-DAMP for 48 h decreased epithelial branching (Figures 2A and B), as previously reported (Knox et al., 2010). However, it did not prevent K19(+) cells from condensing at the ductal midline or affect the distribution of ZO1(+) tight junctions (Figures 2B and C). Indeed, 4-DAMP treated SMG formed narrower elongated ducts with smaller end buds compared to control, as illustrated by time-lapse imaging (Movie S1). Thus, ACh/M1 signaling is not strictly required for ductal tubulogenesis in the developing SMG.

As the loss of functional innervation that results in abnormal ductal tubulogenesis is not recapitulated by muscarinic antagonism (Figures 1D and 2A–C; Movie S1), we speculated that a different neurotransmitter was involved. To identify neurotransmitters and their receptors that might regulate this process, we analyzed an existing microarray data set of the developing SMG (E11-adult; http://sgmap.nidcr.nih.gov/sgmap/sgexp.html). We searched for genes that were upregulated during duct development and/or were co-regulated with the ductal epithelial markers *Krt19, Cldn7* (claudin-7), and *Krt7*. Using this strategy, we found that expression of the VIP receptor, VIPR1, tightly clustered with the ductal markers (Figure 2D). In addition, the ligand for VIPR1, the neuropeptide VIP (Figure 2D), but not other parasympathetic neurotransmitters (NPY, tachykinin and neuropeptide b; data not shown), increased at the initiation of secondary duct formation (E13) and lumenization (E13). Further analysis of the tissue distribution of VIP and VIPR1 expression by qPCR and immunohistochemistry revealed that VIPR1 was highly expressed in the epithelium (Figure

2E and F) and a subpopulation of neuronal cells (data not shown). In contrast, VIP was enriched in the PSG (Figures 2E and F) and absent in epithelial tissue. The absence of VIP from the epithelium was further confirmed by genetic lineage tracing in which VIP-Cre transgenic mice (Taniguchi et al., 2011) were crossed to a $Rosa26^{mTmG}$ reporter strain (Figure 2G). Lastly, we found that expression of *Vip* but not other neuropeptides was significantly increased in the PSG upon NRTN stimulation (~6.1-fold; Figure 2H), suggesting that epithelial NRTN actively promotes VIP secretion by the nerves.

Treatment of SMGs with a specific and well characterized VIPR1 peptide antagonist (VIPR1ant; (Ceraudo et al., 2012; Gourlet et al., 1997); Figures 2A and B); or knockdown of *Vipr1* using siRNA (Figure S2A–D) reduced the number of epithelial branches, similar to treatment with 4-DAMP (Figures 2A and B) or anti-NRTN function blocking antibody (Figure 1B; (Knox et al., 2013)). In contrast to both control and 4-DAMP treated SMG, VIPR1anttreated glands exhibited significantly wider K19(+) ducts (Figures 2B and C) and impaired condensation of K19(+) ductal cells and ZO1(+) tight junctions at the midline (Figure 2C and Figure S2A). This effect was not due to the loss of innervation or neuronal defects, as VIPR1ant treatment did not reduce (or increase) axon outgrowth (Figure 2I and Figure S2E) or neuronal gene expression (Figure 2J).

In addition to increasing expression of genes involved in ACh/muscarinic signaling (*Vacht*, 2-fold), and synapse formation (*Syn2*, 2.6-fold; Figure 2J), 4-DAMP treatment of E13 SMGs caused a striking increase in innervation and VIP protein (Figure 2I, middle panel, yellow and Figure S2E, middle panel) and to a lesser extent *Vip* transcript (1.6-fold, Figure 2J). We speculated that this increase in VIP is responsible for the more ductal appearance of the muscarinic receptor antagonized SMG (Figures 2A–C; Movie S1). This notion prompted us to determine if exogenous VIP could increase duct tubulogenesis. E13 SMGs were treated with VIP for 24h and they resembled the 4-DAMP phenotype: end buds were smaller in size, ducts were narrower, and condensation of K19(+) cells at the ductal midline increased (Figure S2F and G). Together, these data indicate that ductal tubulogenesis in the SMG is regulated by the PSG through a VIP/VIPR1-dependent mechanism.

VIP is sufficient to mediate the effect of the PSG on ductal epithelial growth

To confirm the role of the PSG and VIP in ductal tubulogenesis, we employed epithelial cultures devoid of mesenchyme and nerves (Steinberg et al., 2005). We first tested whether a physical interaction between the epithelium and nerves was required to regulate morphogenesis by co-culturing epithelia with ~4–5 PSG explants placed at a distance from the epithelium. To promote VIP production by the PSG, NRTN was added to the media. Epithelia co-cultured with PSGs displayed increased branching and ductal growth as compared to epithelia cultured alone, indicating that a direct interaction between nerves and epithelium was not required (Figures 3A and B). To determine if VIP produced by PSG was responsible for epithelial morphogenesis we inhibited VIPR1. The VIPR1ant abrogated the effect of the PSG on ductal length but not the number of branches (Figures 3A and B). Interestingly, this was in contrast to the reduced branching observed in intact SMGs cultured with VIPR1ant (Figure 2A and B), suggesting that other neuronal-derived factors may promote epithelial bud formation independently of VIP (Knox et al., 2010).

To confirm that VIP was sufficient to induce ductal growth in the SMG, we treated isolated epithelial rudiments in the absence of nerves with VIP. This mimicked the effect of the PSG on ductal tubulogenesis, causing a significant increase in branch number and ductal length (Figures 3C and E). Furthermore, VIP increased proliferation of cells in ducts by ~2.7-fold over controls, as assayed by EdU incorporation (Figures 3C, D and E). Most of these EdU(+) ductal cells were K19(+) (Figure 3D), indicating that luminal cells are the primary targets of VIP in SMG epithelium. Consistent with this, K19(+) ductal cells expressed VIPR1 (Figure S3). Together, these data demonstrate that VIP from the PSG is sufficient to induce ductal growth in the SMG via expansion of the K19(+) luminal population.

VIP is required for formation of contiguous ductal lumen

A functional duct requires the creation of a contiguous lumen. For several tubular organs, including the salivary gland, epithelial cell polarization results in multiple microlumens that fuse to form a contiguous lumen (Figure 1A, Figure S1B and Movie S2; (Bagnat et al., 2007; Hieda et al., 1996; Kesavan et al., 2009; Walker et al., 2008; Yang et al., 2013). However, the signaling events that elicit formation of a single lumen are not known. We investigated the effect of VIP on cell polarization and lumen formation in the SMG (Figure 3F) by culturing E13 epithelia with exogenous VIP for 48 h. Cell polarity and lumen formation were analyzed using an apical marker atypical protein kinase C (aPKC), GM130 (a Golgi marker with subapical localization) and the epithelial cell-cell adhesion protein E-cadherin (Ecad) as a lateral/basal marker. In the absence of VIP, ductal cells polarized along the ductal axis to form small apical patches or microlumens enriched in aPKC and GM130 (Figures 3G and H, upper panel, arrow heads). However, in the presence of VIP, a contiguous lumen formed, as marked by apical aPKC and subapical GM130 (Figures 3G and H, lower panel). Nuclei staining further confirmed a single lumen in VIP-treated epithelia (Figure 3G). Thus, while ductal cells can polarize and form microlumens in the absence of VIP, the formation of a single contiguous lumen requires VIP.

VIP promotes ductal growth and lumen formation in a cAMP-dependent manner

VIPR1 belongs to the Gs protein-coupled class of receptors, whose activation results in elevation of cAMP and subsequent activation of cAMP-dependent protein kinase A (PKA). Therefore we asked if VIP coordinates tubulogenesis in a cAMP/PKA-dependent manner. Treatment of epithelial rudiments with VIP increased cAMP and phosphorylation of the PKA target cAMP Response Element-Binding protein (CREB; Figures 4A and B). Supporting the role of cAMP in ductal tubulogenesis, the membrane-permeable cAMP analog, 8-bromoadenosine-3,5-cyclic monophosphate (8-Br-cAMP), mimicked the effect of VIP on epithelial ductal growth (Figures 4C and D) and induced formation of a contiguous lumen, with apical enrichment of F-actin and subapically located GM130 (Figure 4D). Moreover, the selective PKA inhibitor Rp-CPT-cAMPS abrogated both VIP-mediated ductal elongation in epithelial rudiment culture (Figure S4A and B) and lumen formation in intact salivary gland explants (containing PSG), as highlighted by the luminal marker prominin-1 (Prom1; Figure 4E). Thus, VIP regulates ductal growth and formation of a contiguous lumen via cAMP/PKA signaling.

VIP-induced lumen formation does not require apoptosis

Apoptosis is a potential mechanism for lumen formation in several glandular organs including mammary and salivary glands (Humphreys, 1996; Mailleux, 2007). To determine whether apoptosis mediates VIP-dependent lumen formation in salivary glands, we inhibited apoptosis by culturing E13.5 SMGs with the pan-caspase inhibitor Z-VAD-FMK for 24h (Figure S4A and B). Consistent with previous reports for cultured SMG (Hoffman, 2002; Walker, 2008; Patel, 2011), apoptosis occurs in the mesenchyme, with few apoptotic cells within the branching epithelium (or lumens; Figure 5A and B). In the presence of Z-VAD-FMK, mesenchymal and epithelial cell death was not observed (Figure 5B), yet epithelial lumens formed and were similar to the untreated SMG (Figure 5A). To confirm that apoptosis did not mediate lumen formation in SMGs in vivo, we assessed the ductal system of SMG derived from E17 mice deficient in the pro-apoptotic factor, Bax. *Bax*-null SMGs were phenotypically normal, with a tubular ductal system similar to wild type controls (Figure 5C). Thus, from these studies we conclude that VIP-mediated lumen formation in the SMG is not dependent on apoptosis.

VIP rapidly expands ductal lumens in a cAMP/PKA- and CFTR-dependent manner

After a nascent lumen is formed, it must expand for fluid transport. Multiple mechanisms of lumen expansion have been identified including solutes and water transport, secretion of luminal matrix or polarized vesicular transport (rev. in (Datta et al., 2011). Because VIP enlarges lumens of spherical epithelial cysts *in vitro* (Talbot et al., 2002), we asked whether VIP also regulates lumen expansion in the SMG. VIP treatment of SMG explants led to a rapid expansion of the primary duct lumen compared to the untreated control (asterisks in Figure S2F, and arrowheads in Figure S5A). Because the primary duct already contains a mature lumen when the gland is isolated for *ex vivo* culture, these data indicate that VIP regulated lumen expansion directly, independently of its polarizing effect on ductal cells.

To further test whether VIP-mediated lumen expansion was independent of its effects on growth and lumen formation, we modified our epithelial rudiment culture to exclude the effect of VIP on these parameters. Epithelia were cultured for 28–30 h in the presence of HBEGF, which increases duct cell proliferation (Knox et al., 2010) and promotes formation of elongated secondary ducts with multiple microlumens (Figure 6A). Importantly, despite its prominent effect on ductal growth, HBEGF was not able to promote formation of a single contiguous lumen. To study the role of VIP in lumen expansion, epithelia were then treated with and without VIP as well as agonists and antagonists of PKA for 1 h (Figure 6A). Both VIP and the cAMP analog, 8-CPT-cAMP, initiated the expansion of microlumens, which partially coalesced to form larger lumens (Figure 6B and Figure S5B). In contrast, the ACh analog carbachol (CCh), which does not increase cAMP, did not induce lumen expansion (Figure S5B). Further experiments demonstrated that VIP-induced lumen expansion requires activation of PKA. First, VIP-induced lumen expansion was abolished by the PKA inhibitor, Rp-CPT-cAMPS (Figure 6B and Figure S5B). Second, 8-pCPT-2’-O-Me-cAMP, a selective activator of another major cAMP-target, the Exchange protein directly activated by cAMP (Epac), did not induce lumen expansion, while structurally similar 8-CPT-cAMP, which activates both PKA and Epac, did (Figure 6B and Figure S5B). Together these data indicate

that cAMP/PKA-dependent signaling is required and sufficient for lumen expansion and that the effect of VIP on lumen expansion is not only due to its mitogenic role in duct elongation.

PKA regulates lumen expansion through increased flow of electrolytes and fluid transport (Bagnat et al., 2010; Jaffe et al., 2008), as well as apoptosis of luminal cells (Nedvetsky et al., 2012). Using live cell imaging of epithelia labeled with membrane-bound RFP, we observed luminal cavities that appear and expand within 10 min of adding VIP (Figure 6C). The fast nature of lumen expansion and the lack of isolated cells (Figure 6B) or cleaved caspase 3(+) apoptotic cells (data not shown) within newly forming lumens (<1 h), suggested that lumen expansion was driven by electrolyte and fluid flow rather than apoptosis. We identified CFTR as a likely candidate as it regulates cAMP-dependent lumen expansion in zebrafish (Bagnat et al., 2010); VIP enhances CFTR activity and localization at the apical membrane of epithelial cells (Chappe et al., 2008; Qu et al., 2011); and CFTR protein is enriched in SMG ducts at the presumptive lumen during development (Figures S5C and D). Upon inhibition of CFTR using the specific inhibitor CFTRinh-172, VIP-mediated lumen expansion was inhibited to a similar extent as the PKA inhibitor, Rp-CPT-cAMPS (Figure 6B and Figure S5B). Importantly, the presence of CFTRinh-172 did no affect the polarization of ductal cells and formation of contiguous lumen (Figure S5E). Thus, VIP/VIPR1 promotes lumen formation and expansion through different mechanisms with the CFTR-dependent pathway involved in lumen expansion but not lumen formation.

VIP-dependent innervation coordinates SMG tubulogenesis in vivo

Next, we tested whether VIP(+) parasympathetic nerves coordinates SMG tubulogenesis *in vivo* using mice deficient in the nerve-derived factor neuregulin 1 type III (*Nrg1-III* ; (Wolpowitz et al., 2000)). These mice show depleted innervation of numerous tissues, dying from respiratory failure at birth. Nrg1-III deficient salivary glands were devoid of functional nerves and exhibited aberrant ductal morphogenesis: epithelial branching was reduced (Figure 7A and B) with disrupted lumen formation (Figure 7A, ZO1 immunostaining, lower panel) and expansion (Figure 7D and F, arrows). We next asked whether this phenotype was due to loss of FGF10/FGFR2b signaling, an essential regulator of epithelial branching in the SMG (Jaskoll et al., 2005). However, expression of *Fgf10* and FGFR2b targets, *Etv4* and *5*, were unchanged (Figure 7C). In addition, reduction of FGF10/FGFR2b signaling *ex vivo* (Figure S6A (Steinberg et al., 2005)) or *in vivo* (Figure S6B; (Jaskoll et al., 2005)) had no effect on ductal development. Together, these data indicate that deficient VIP-dependent innervation results in impaired SMG tubulogenesis *in vivo*.

To determine whether reduced VIP/VIPR1 signaling decreased tubulogenesis similar to that observed in the absence of parasympathetic nerves *in vivo* (Figure 7A and D), we inhibited VIPR1 during in vivo SMG development (E12–E16) using the VIPR1 antagonist. Pregnant mice were injected with VIPRant between E12 and E16, as described previously (Gressens et al., 1994; Passemard et al., 2011) and lumen formation was analyzed at E17.5. Strikingly, the luminal cavities of salivary glands from VIPRant-treated embryos were smaller than those of the glands from control embryos (PBS only; Figure 7E and G), confirming that VIP is necessary for lumen expansion. We did not find lumen formation to be disrupted (data not shown). However, this may be due to the concentration of VIPR1ant being too low to inhibit

this process or additional factors compensate for VIPR1 inhibition. Lastly, we asked if CFTR was required for tubulogenesis *in vivo* using SMG derived from *Cftr* deficient mice (Snouwaert et al., 1992). Compared to wild type controls, *Cftr*-null SMG exhibited aberrant tubulogenesis as shown by the absence of large granulated ducts (Figure 6H; see arrow in wild type), thus confirming a role for CFTR in epithelial tubulogenesis in the SMG.

Discussion

Previous studies of tubulogenesis have highlighted a role of multiple molecular pathways (rev. by (Iruela-Arispe and Beitel, 2013)). However, mechanisms coordinating morphogenic processes during tubulogenesis are poorly understood. Our data reveal that parasympathetic nerves serve to coordinate epithelial tubulogenesis in the developing salivary gland. We demonstrate that the neurotransmitter VIP and its receptor VIPR1 regulate multiple steps during epithelial tubulogenesis that include cell proliferation, duct elongation, lumen formation and lumen expansion (Figure 7I; (Knox et al., 2010), thus linking epithelial tubulogenesis with parasympathetic neuronal function. Lastly, we identify a potential mechanism whereby NRTN produced by the epithelium promotes functional nerve outgrowth to ensure parallel development of nerves and epithelium (Figure 7I).

Our studies also demonstrate that VIP and ACh have essential, non-overlapping functions during duct formation. Proliferation of basal epithelial progenitor cells necessary for epithelial branching requires ACh/M1/EGFR signaling (Knox et al., 2010). Other pathways, such as HBEGF/EGFR, promote luminal cell proliferation and differentiation during duct development (Figure 6H; (Haara et al., 2009; Knox et al., 2010), but do not compensate in the absence of functional innervation. Therefore, we propose HBEGF/EGFR to act in concert with parasympathetic signals during ductal tubulogenesis but that ACh and VIP are key regulators of events necessary to create a functional tubular network (Figure 7I).

Our study also provides an answer to one of the puzzling questions in the field of epithelial tubulogenesis: what factors orchestrate the formation of a contiguous lumen. Microlumen formation relies on the intrinsic ability of epithelial cells to polarize (Sternlicht et al., 2006), but the signaling events controlling microlumen fusion to establish a common single lumen are just beginning to emerge (Iruela-Arispe and Beitel, 2013). Our study indicates that, at least in the SMG, transition from multiple microlumens to a single contiguous lumen requires the external neuronal factor VIP. Since this process of lumenization also occurs in other epithelial tissues innervated by VIP-secreting nerves, such as the pancreas, kidney and intestine (Bagnat et al., 2007; Kesavan et al., 2009; Yang et al., 2013), VIP-dependent innervation may also regulate formation of a contiguous lumen in these organs.

We also show that VIP(+) nerves activate PKA during development to regulate multiple steps during ductal tubulogenesis. Pharmacological manipulations of PKA have been shown to affect epithelial cell polarity and morphogenesis *in vitro* (Nedvetsky et al., 2012; Tee et al., 2010). However, we identify an endogenous upstream signal engaging PKA in the regulation of epithelial tubulogenesis. What remains to be determined is the identity of the signaling molecules downstream of VIP/VIPR1/PKA that promote the formation of a contiguous lumen from multiple discontinuous microlumens. One potential candidate for

this process is the Hedgehog signaling pathway. Exogenous Shh promotes lumen formation in cultured SMG (Hashizume and Hieda, 2006) and the Shh receptor smoothened regulates coalescence of microlumens in developing zebrafish gut (Alvers et al., 2014). In this study Shh acts on the mesenchyme and not the epithelium leading the authors to propose signaling from the mesenchyme supports tubulogenesis. Whether Shh regulates production of VIP, which is expressed by the nerves within the mesenchymal compartment, or functions downstream of VIP/VIPR1 remains to be seen.

The role of apoptosis in salivary gland lumen formation has been a matter of debate. Previous studies show cleaved caspase-3(+) cells within luminal duct regions of isolated SMGs (Wells and Patel, 2010). However, conclusive evidence demonstrating a link between apoptosis and lumen formation has not been reported. Our findings argue against an essential role of apoptosis in lumen formation or expansion in the SMG and support the hypothesis that the formation of a contiguous ductal network is independent of apoptosis in the developing salivary gland.

Similar to what has been observed for cAMP-mediated lumen expansion in zebrafish gut development (Bagnat et al., 2007), we found lumen expansion to be dependent at least in part, on a VIP-responsive PKA/CFTR-dependent mechanism. Reduced lumen expansion and/or atresia of the intestine have been found in *Vip*-, *Vipr1*- and *Cftr*-null animals (Fabricius et al., 2011; Hodges et al., 2008; Lelievre et al., 2007; Meyerholz et al., 2010). Similarly, we show that formation of the ductal network in salivary gland derived from *Cftr*-null mice is impaired (Figure 7H). As *Cftr*, *Vip* and *Vipr1* are inactivated in all tissues, aberrant epithelial tubulogenesis may be a consequence of other events. However, our data support a direct role of VIP and CFTR in ductal lumen expansion. It remains to be determined how CFTR activity results in lumen expansion in the SMG. Given both PKA and CFTR promote fluid secretion in developing and adult tissues (Bagnat et al., 2010; Magenheimer et al., 2006; Seino and Shibasaki, 2005), we predict that fluid secretion mediated by VIP/PKA/CFTR also accounts for lumen expansion in the developing salivary gland.

In summary, we have identified parasympathetic nerves and specifically VIP and its downstream effectors PKA and CFTR as key regulators of epithelial tubulogenesis during salivary gland development. We find lumen formation and lumen expansion in SMG ducts to be regulated independently. While both lumen formation and expansion required VIP/cAMP/PKA-dependent signaling, only lumen expansion involves CFTR activity. Consequently, parasympathetic nerves function in two distinct processes of SMG tubulogenesis: lumen formation and lumen expansion. Such findings have significant implications for the repair, regeneration and/or de novo generation of branching organs, where efficient transport of fluid and osmolates through an interconnected ductal system is vital to organ function (Aframian and Palmon, 2008). Lastly, our data establishes the parasympathetic nervous system as an important player in epithelial tubulogenesis during organogenesis, highlighting the multifunctional contribution of nerves to developmental processes.

Materials and Methods

Mouse lines, breeding, and genotyping

Strains used on this study include: C+D1 (Harlan, CA), Nrg1^{tm1Lwr} (targeted mutation in Nrg1 type III; provided by Dr. Lorna Role, NYU, NY; (Wolpowitz et al., 2000)), Vip$^{tm1(cre)Zjh}$ (Vip-Cre) was provided by Dr. John Rubenstein, UCSF, CA (Taniguchi et al., 2011); Gt(Rosa)26Sor$^{tm4(ACTB-tdTomato,-EGFP)Luo}$ (*Rosa26*^{mTmG} (Muzumdar et al., 2007)) were from Dr. Ophir Klein, UCSF, CA; and Bax^{tm1Sjk} was provided by Dr. Diana Laird, UCSF, CA (Knudson et al., 1995)) and Cftr^{tm1Unc} (Snouwaert et al., 1992). All experiments were approved by the Institutional Animal Care and Use Committee at UCSF. For timed-matings the morning of plug detection was considered day 0.5 post-coitum. For lineage tracing, *Vip-Cre* mice were crossed with *Rosa26*^{mTmG} reporter mice to obtain salivary glands from embryonic day 14 and post-natal day 1 pups. Genotyping of mice was performed on tail biopsies by PCR and agarose gel electrophoresis using specific primers.

SMG organ culture

SMG explants were cultured as previously described (Steinberg et al., 2005). Briefly, freshly dissected SMG were plated on nucleopore filters over medium containing glucagon (control, 30 μM, Anaspec) or, when indicated, VIPR1 peptide antagonist (30 μM; Pheonix Pharmaceuticals), the pan-caspase inhibitor Z-VAD-FMK (50μM; Tocris; Minneapolis, MN, US); 1,1-Dimethyl-4-diphenylacetoxypiperidinium iodide (4-DAMP; 10 μM; muscarinic receptor inhibitor; Tocris, MN) or Rp-8-CPT-cAMPS (“Rp”; 50 μM, PKA inhibitor, Biolog, Bremen, Germany) for 24 or 48 h. Explants were either lysed for RNA or fixed for immunostaining.

Epithelial rudiment cultures

SMGs were harvested from E13 ICR mice, the epithelia were separated from mesenchyme using dispase treatment and mechanical dissection and epithelial rudiments cultured in a 15 μL drop of laminin-1,1,1 (Trevigen) on nucleopore filters floating above serum free medium (Steinberg et al., 2005). All epithelial assays contain 400 ng/mL FGF10 (R&D Systems, Minneapolis, MN, US) and 0.5 μg/mL heparan sulfate (Sigma, MO, USA).

To study ductal growth and lumen formation, epithelia were also cultured with 200 nM VIP (Anaspec) or 20 μM 8-bromoadenosine-3, 5 -cyclic monophosphate (8-Br-cAMP, Sigma). For lumen expansion assays, epithelia were cultured with FGF10 and 10 ng/ml HBEGF (R&D Systems, MN) for 28 h before the addition of 200μM 8-CPT-cAMP (“CPT”; PKA/Epac activator, Biolog), 200 μM 8-pCPT-2’-O-Me-cAMP (“007”; Epac activator, Biolog), 200 nM carbachol (CCh, Sigma), or 200 nM VIP with or without 250 μM Rp-8-CPT-cAMPS (“Rp”; PKA inhibitor, Biolog), 10–40 μM CFTR172 (Sigma, MO) or 5 μM PD168393 (EGFR inhibitor, Tocris). Epithelia were cultured another hour before fixation for immunostaining.

For PSG/epithelia co-cultures, PSGs were separated from E13 SMG as for epithelia above. ~4–5 PSGs were placed in the center of the drop of laminin-1,1,1 and epithelia were placed <1mm from the PSGs. The neurotrophic growth factor neurturin (10 ng/mL; R&D systems,

MN) was added to the media to support neuronal growth and VIP expression by the PSGs (Knox et al., 2013).

In vivo inhibition of VIP receptor

VIPR antagonist ([D-p-Cl-Phe^6, Leu^{17}]-VIP; Tocris, MN) was injected into timed pregnant CD1 mice as described previously (Gressens et al., 1994; Passemard et al., 2011). CD1 timed pregnant females were injected with 1.2 μg per gram of body weight of VIP antagonist or PBS (200 μL; solvent for VIPR antagonist) twice daily for 5 consecutive days (E12–E16). E17.5 salivary glands were collected, fixed and stained, as indicated below.

Quantitative PCR analysis (qPCR)

Total RNA samples were DNase treated (Ambion, Austin, TX), prior to cDNA synthesis using SuperScript reagents (Invitrogen, CA). SYBRgreen qPCR was performed using 1 ng of cDNA, and primers designed using Beacon Designer software. See Table S1 in Supplementary Experimental Procedures for primer sequences.

Melt-curves and primer efficiency were determined as previously described (Hoffman et al., 2002). Gene expression was normalized to *29S* (Rsp29) and to the corresponding experimental control. Reactions were run in triplicate and repeated three times.

Immunofluorescence analysis

Whole-mount immunofluorescence analysis has been described (Knox et al., 2010). Briefly, SMG and epithelia were fixed with either ice-cold acetone/methanol (1:1) for 5 min or 4% paraformaldehyde (PFA) for 20 min followed by 0.1% Triton-X100/PBS for 10 min. For analysis of SMG older than E16, after fixation with 4% PFA glands were embedded in OCT and frozen tissue sections of 15–30 μm were analyzed. Tissue was blocked 4 h at 22°C with 10% Donkey Serum (Jackson Laboratories, ME), 1% BSA, and MOM IgG-blocking reagent (Vector Laboratories, CA) in 0.01% PBS-Tween-20. SMG or epithelia were incubated with primary antibodies overnight at 4°C: mouse anti-GM130 (1:500, BD Biosciences), rabbit anti-ZO1 (1:100, Invitrogen), rat anti-prominin-1 (1:200, Biolegends), rabbit anti-aPKC (C-20, 1:400, Santa Cruz Biotech Ltd), mouse anti-Tubb3 (clone TUJ1 at 1:400; R&D Systems); rat anti-Ecadherin (1:400; clone ECCD-2; Invitrogen); rabbit anti-cleaved caspase-3 (5A1E, 1:200, Cell Signaling); or rat anti-Krt19 (1:300; tromaIII, DSHB). Antibodies were detected using Cy2-, Cy3- or Cy5-conjugated secondary Fab fragment antibodies (Jackson Laboratories). F-actin was detected with Alexa Fluor 488® or Rhodamine phalloidin (1:50; Invitrogen). Fluorescence was analyzed using a Leica Sp5 microscope and NIH ImageJ software.

Cell proliferation was detected using Click-iT EdU Imaging Systems (Invitrogen, CA) as described by the manufacturer. Briefly, SMG or epithelia were cultured with EdU (5μM) for 30 min, fixed with 1:1 ice-cold acetone/methanol, and then incubated with Click-iT EdU reaction cocktail for 30 min. EdU(+) cells were counted in the duct regions of individual epithelia and normalized to total number of Dapi(+) nuclei and expressed as fold increase compared to control conditions.

cAMP assay and western blotting

For cAMP assay, epithelia were pre-incubated with IBMX (200μM) before the addition of 10–500nM VIP. After 1 h, epithelia were lysed in 150 μL lysis buffer from the commercial enzyme-linked immunoassay kit (Cyclic AMP XP Assay kit; Cell Signaling) and cAMP was measured according to the manufacturer's instructions.

Phosphorylation of CREB was assessed via Western blotting. E13 epithelia cultured for 24 h and thereafter treated with VIP (100–1000 nM) for 15 min. Epithelia were lysed directly in 250 μl Laemmli buffer. Proteins were separated by SDS-PAGE, transferred onto the polyvinylidene fluoride membrane, and immunoblotted with specific antibodies for CREB and phospho-CREB (Cell Signaling).

Live cell imaging

Epithelia were cultured with VIP and HBEGF for 28 h as above. Filters were inverted and placed into 3.5 cm glass bottom dishes (MatTek). VIP (200 nM) was added to the media at the beginning of imaging. Imaging was performed on a custom-build inverted spinning disc confocal microscope based on a Nikon TI microscope stand, equipped with environmental control (In Vivo Scientific), a Boralis-modified Yokogawa CSU-X1 confocal head and LMM5 laser merge module (both from Spectral Applied Research), motorized stage (Applied Scientific Instruments) and perfect focus system (Nikon) (Stehbens et al., 2012)). Samples were illuminated with a 100 mW 561 nm solid state laser (Cobolt Jive) and imaged using a Nikon CFI Plan Apo N.A. 1.2 60× water immersion objective and Andor Clara CCD camera. Image acquisition was controlled by Nikon Elements software. Optical sections were taken every 1 μm over the entire specimen at 100 ms exposure per plane and 2 minute intervals. Frames were selected and z-axis reconstructions prepared with the ImageJ/Fiji (http://fiji.sc/Fiji).

Morphometric and statistical analyses

Morphogenesis was quantified by counting the number of branches or duct length. All SMG data were obtained using 4–5 SMGs/group and each experiment repeated three times. Data were log transformed before all statistical analysis with GraphPad Prism 6 software (GraphPad Software Inc., CA). The Student's **t**-test was used to compare two different groups and one-way analysis of variance to compare more than two experimental groups. For qPCR analysis, a false discovery rate (*Q*) for multiple unpaired t-tests was set to 5%. All graphs show the means ± standard deviation (SD).

Supplementary Material

Refer to Web version on PubMed Central for supplementary material.

Acknowledgments

We thank Drs. Ann Zovein, Ophir Klein, Jeff Bush, David Bryant, Volker Henn, Ross Metzger, and Li-Kun Phng for critical reading of the manuscript. This work was supported by National Institutes of Health (NIH) grants 5R00DE018969 and R21DE022951 to S.M.K. and 5R01DK074398 and 5R01DK091530 to K.E.M. Research was conducted on a spinning disc microscope system funded by Shared Equipment Grant S10 RR26758 from the National Center for Research Resources of the National Institutes of Health.

References

Aframian DJ, Palmon A. Current status of the development of an artificial salivary gland. Tissue Eng. Part B. Rev. 2008; 14:187–198. [PubMed: 18471085]

Alvers AL, Ryan S, Scherz PJ, Huisken J, Bagnat M. Single continuous lumen formation in the zebrafish gut is mediated by smoothened-dependent tissue remodeling. Development. 2014; 141:1110–1119. [PubMed: 24504339]

Bagnat M, Cheung ID, Mostov KE, Stainier DY. Genetic control of single lumen formation in the zebrafish gut. Nat. Cell Biol. 2007; 9:954–960. [PubMed: 17632505]

Bagnat M, Navis A, Herbstreith S, Brand-Arzamendi K, Curado S, Gabriel S, Mostov K, Huisken J, Stainier DY. Cse1l is a negative regulator of CFTR-dependent fluid secretion. Curr. Biol. : CB. 2010; 20:1840–1845.

Ceraudo E, Hierso R, Tan YV, Murail S, Rouyer-Fessard C, Nicole P, Robert JC, Jamin N, Neumann JM, Robberecht P, et al. Spatial proximity between the VPAC1 receptor and the amino terminus of agonist and antagonist peptides reveals distinct sites of interaction. FASEB J. 2012; 26:2060–2071. [PubMed: 22291440]

Chappe F, Loewen ME, Hanrahan JW, Chappe V. Vasoactive intestinal peptide increases cystic fibrosis transmembrane conductance regulator levels in the apical membrane of Calu-3 cells through a protein kinase C-dependent mechanism. J. Pharmacol. Exp. Ther. 2008; 327:226–238. [PubMed: 18650246]

Coughlin MD. Early development of parasympathetic nerves in the mouse submandibular gland. Dev. Biol. 1975; 43:123–139. [PubMed: 1149921]

Datta A, Bryant DM, Mostov KE. Molecular regulation of lumen morphogenesis. Curr. Biol. 2011; 21:R126–R136. [PubMed: 21300279]

Fabricius D, Karacay B, Shutt D, Leverich W, Schafer B, Takle E, Thedens D, Khanna G, Raikwar S, Yang B, et al. Characterization of intestinal and pancreatic dysfunction in VPAC1-null mutant mouse. Pancreas. 2011; 40:861–871. [PubMed: 21697765]

Gourlet P, De Neef P, Cnudde J, Waelbroeck M, Robberecht P. In vitro properties of a high affinity selective antagonist of the VIP1 receptor. Peptides. 1997; 18:1555–1560. [PubMed: 9437716]

Gressens P, Hill JM, Paindaveine B, Gozes I, Fridkin M, Brenneman DE. Severe microcephaly induced by blockade of vasoactive intestinal peptide function in the primitive neuroepithelium of the mouse. J. Clin. Invest. 1994; 94:2020–2027. [PubMed: 7962548]

Haara O, Koivisto T, Miettinen PJ. EGF-receptor regulates salivary gland branching morphogenesis by supporting proliferation and maturation of epithelial cells and survival of mesenchymal cells. Differentiation. 2009; 77:298–306. [PubMed: 19272528]

Hashizume A, Hieda Y. Hedgehog peptide promotes cell polarization and lumen formation in developing mouse submandibular gland. Biochem. Biophys. Res. Comm. 2006; 339:996–1000. [PubMed: 16332353]

Hieda Y, Iwai K, Morita T, Nakanishi Y. Mouse embryonic submandibular gland epithelium loses its tissue integrity during early branching morphogenesis. Dev. Dyn. 1996; 207:395–403. [PubMed: 8950514]

Hodges CA, Cotton CU, Palmert MR, Drumm ML. Generation of a conditional null allele for Cftr in mice. Genesis. 2008; 46:546–552. [PubMed: 18802965]

Hoffman MP, Kidder BL, Steinberg ZL, Lakhani S, Ho S, Kleinman HK, Larsen M. Gene expression profiles of mouse submandibular gland development: FGFR1 regulates branching morphogenesis in vitro through BMP- and FGF-dependent mechanisms. Development. 2002; 129:5767–5778. [PubMed: 12421715]

Iruela-Arispe ML, Beitel GJ. Tubulogenesis. Development. 2013; 140:2851–2855. [PubMed: 23821032]

Jaffe AB, Kaji N, Durgan J, Hall A. Cdc42 controls spindle orientation to position the apical surface during epithelial morphogenesis. J. Cell Biol. 2008; 183:625–633. [PubMed: 19001128]

Jaskoll T, Abichaker G, Witcher D, Sala FG, Bellusci S, Hajihosseini MK, Melnick M. FGF10/FGFR2b signaling plays essential roles during in vivo embryonic submandibular salivary gland morphogenesis. BMC Dev. Biol. 2005; 5:11. [PubMed: 15972105]

Kang JH, Kim BK, Park BI, Kim HJ, Ko HM, Yang SY, Kim MS, Jung JY, Kim WJ, Oh WM, et al. Parasympathectomy induces morphological changes and alters gene-expression profiles in the rat submandibular gland. Arch. Oral Biol. 2010; 55:7–14. [PubMed: 20003962]

Kesavan G, Sand FW, Greiner TU, Johansson JK, Kobberup S, Wu X, Brakebusch C, Semb H. Cdc42-mediated tubulogenesis controls cell specification. Cell. 2009; 139:791–801. [PubMed: 19914171]

Knox SM, Lombaert IM, Haddox CL, Abrams SR, Cotrim A, Wilson AJ, Hoffman MP. Parasympathetic stimulation improves epithelial organ regeneration. Nat. Comm. 2013; 4:1494.

Knox SM, Lombaert IM, Reed X, Vitale-Cross L, Gutkind JS, Hoffman MP. Parasympathetic innervation maintains epithelial progenitor cells during salivary organogenesis. Science. 2010; 329:1645–1647. [PubMed: 20929848]

Knudson CM, Tung KS, Tourtellotte WG, Brown GA, Korsmeyer SJ. Bax-deficient mice with lymphoid hyperplasia and male germ cell death. Science. 1995; 270:96–99. [PubMed: 7569956]

Kyriacou K, Garrett JR. Morphological changes in the rabbit submandibular gland after parasympathetic or sympathetic denervation. Arch. Oral Biol. 1988; 33:281–290. [PubMed: 3165263]

Lelievre V, Favrais G, Abad C, Adle-Biassette H, Lu Y, Germano PM, Cheung-Lau G, Pisegna JR, Gressens P, Lawson G, et al. Gastrointestinal dysfunction in mice with a targeted mutation in the gene encoding vasoactive intestinal polypeptide: a model for the study of intestinal ileus and Hirschsprung's disease. Peptides. 2007; 28:1688–1699. [PubMed: 17606312]

Lubarsky B, Krasnow MA. Tube morphogenesis: making and shaping biological tubes. Cell. 2003; 112:19–28. [PubMed: 12526790]

Magenheimer BS, St John PL, Isom KS, Abrahamson DR, De Lisle RC, Wallace DP, Maser RL, Grantham JJ, Calvet JP. Early embryonic renal tubules of wild-type and polycystic kidney disease kidneys respond to cAMP stimulation with cystic fibrosis transmembrane conductance regulator/Na(+),K(+),2Cl(−) Co-transporter-dependent cystic dilation. J. Am. Soc. Nephrol. 2006; 17:3424–3437. [PubMed: 17108316]

Mandour MA, Helmi AM, El-Sheikh MM, El-Garem F, El-Ghazzawi E. Effect of tympanic neurectomy on human parotid salivary gland. Histopathologic, Histochemical, and Clinical Study. Arch. Otolaryngol. 1977; 103:338–341. [PubMed: 869767]

Meyerholz DK, Stoltz DA, Pezzulo AA, Welsh MJ. Pathology of gastrointestinal organs in a porcine model of cystic fibrosis. Am. J. Path. 2010; 176:1377–1389.

Muzumdar MD, Tasic B, Miyamichi K, Li L, Luo L. A global double-fluorescent Cre reporter mouse. Genesis. 2007; 45:593–605. [PubMed: 17868096]

Nedvetsky PI, Kwon SH, Debnath J, Mostov KE. Cyclic AMP regulates formation of mammary epithelial acini in vitro. Molecular biology of the cell. 2012; 23:2973–2981. [PubMed: 22675028]

Passemard S, Sokolowska P, Schwendimann L, Gressens P. VIP-induced neuroprotection of the developing brain. Curr. Pharm. Design. 2011; 17:1036–1039.

Proctor GB, Carpenter GH. Regulation of salivary gland function by autonomic nerves. Autonomic Neuro. 2007; 133:3–18.

Qu F, Liu HJ, Xiang Y, Tan YR, Liu C, Zhu XL, Qin XQ. Activation of CFTR trafficking and gating by vasoactive intestinal peptide in human bronchial epithelial cells. J. Cell. Biochem. 2011; 112:902–908. [PubMed: 21328463]

Seino S, Shibasaki T. PKA-dependent and PKA-independent pathways for cAMP-regulated exocytosis. Physiolog. Rev. 2005; 85:1303–1342.

Stehbens S, Pemble H, Murrow L, Wittmann T. Imaging intracellular protein dynamics by spinning disk confocal microscopy. Methods Enzymol. 2012; 504:293–313. [PubMed: 22264541]

Steinberg Z, Myers C, Heim VM, Lathrop CA, Rebustini IT, Stewart JS, Larsen M, Hoffman MP. FGFR2b signaling regulates ex vivo submandibular gland epithelial cell proliferation and branching morphogenesis. Development. 2005; 132:1223–1234. [PubMed: 15716343]

Sternlicht MD, Kouros-Mehr H, Lu P, Werb Z. Hormonal and local control of mammary branching morphogenesis. Differentiation. 2006; 74:365–381. [PubMed: 16916375]

Talbot NC, Caperna TJ, Wells KD. The PICM-19 cell line as an in vitro model of liver bile ductules: effects of cAMP inducers, biopeptides and pH. Cells, Tissues, Organs. 2002; 171:99–116. [PubMed: 12097833]

Taniguchi H, He M, Wu P, Kim S, Paik R, Sugino K, Kvitsiani D, Fu Y, Lu J, Lin Y, et al. A resource of Cre driver lines for genetic targeting of GABAergic neurons in cerebral cortex. Neuron. 2011; 71:995–1013. [PubMed: 21943598]

Tee JB, Choi Y, Shah MM, Dnyanmote A, Sweeney DE, Gallegos TF, Johkura K, Ito C, Bush KT, Nigam SK. Protein kinase A regulates GDNF/RET-dependent but not GDNF/Ret-independent ureteric bud outgrowth from the Wolffian duct. Dev. Biol. 2010; 347:337–347. [PubMed: 20816800]

Walker JL, Menko AS, Khalil S, Rebustini I, Hoffman MP, Kreidberg JA, Kukuruzinska MA. Diverse roles of E-cadherin in the morphogenesis of the submandibular gland: insights into the formation of acinar and ductal structures. Dev. Dyn. 2008; 237:3128–3141. [PubMed: 18816447]

Wells KL, Patel N. Lumen formation in salivary gland development. Front. Oral Biol. 2010; 14:78–89. [PubMed: 20428012]

Wolpowitz D, Mason TB, Dietrich P, Mendelsohn M, Talmage DA, Role LW. Cysteine-rich domain isoforms of the neuregulin-1 gene are required for maintenance of peripheral synapses. Neuron. 2000; 25:79–91. [PubMed: 10707974]

Yang Z, Zimmerman S, Brakeman PR, Beaudoin GM 3rd, Reichardt LF, Marciano DK. De novo lumen formation and elongation in the developing nephron: a central role for afadin in apical polarity. Development. 2013; 140:1774–1784. [PubMed: 23487309]

Highlights

- Parasympathetic nerves regulate ductal tubulogenesis in the salivary gland
- VIP/VIPR1 signaling guides formation of a contiguous lumen
- VIP regulates duct growth, formation and expansion of lumen via cAMP/PKA signaling
- Lumen formation is independent of apoptosis and involves CFTR

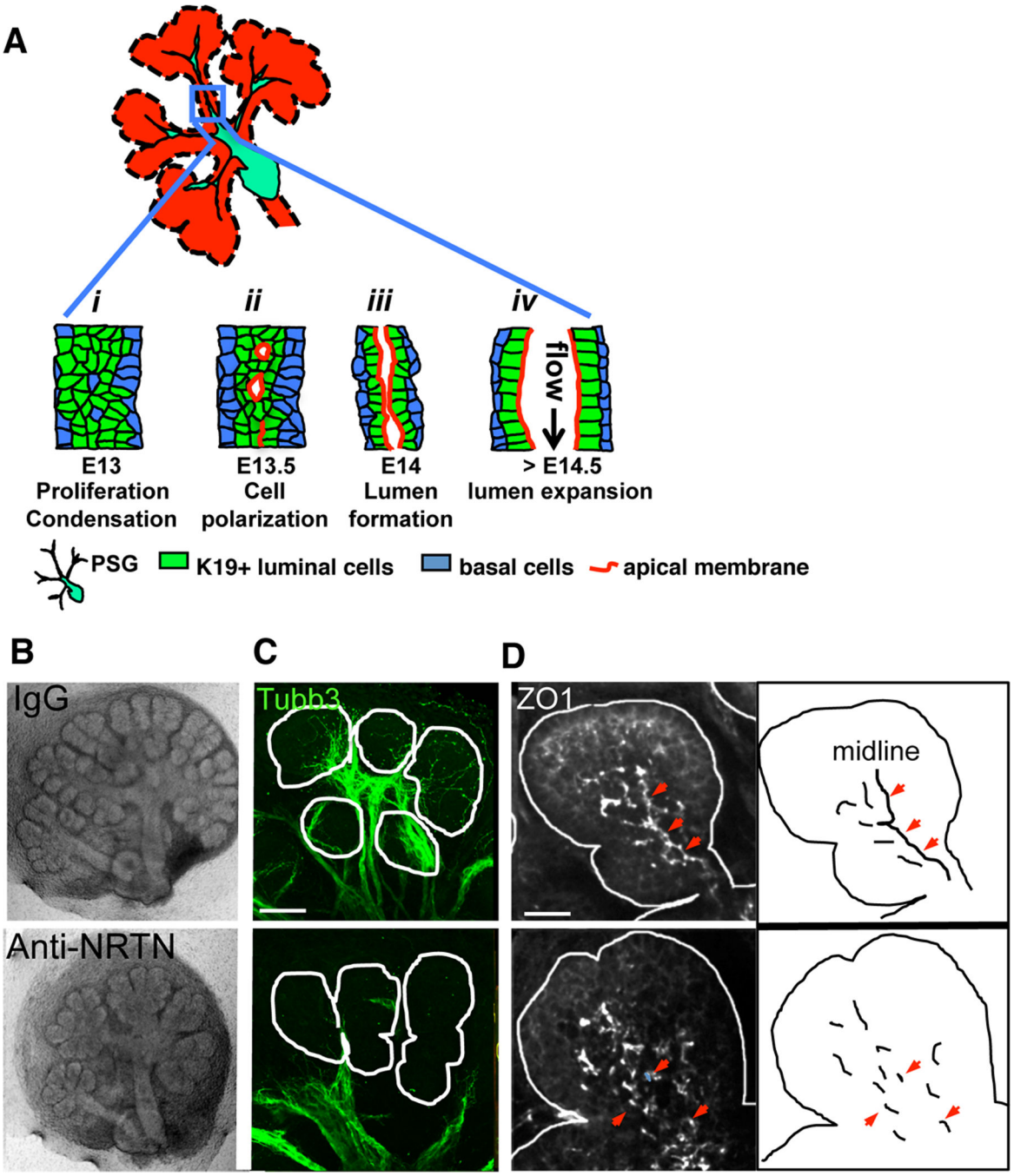

Figure 1. Parasympathetic innervation regulates lumen formation in the SMG

(**A**) Schematic illustration of steps during SMG duct development: ***i***, K19(+) luminal cells condense at ductal midline; ***ii***, cells polarize to form microlumens with shared apical membrane; ***iii***, microlumens coalesce to form a contiguous apical membrane bounding a luminal space; ***iv***, lumen undergoes expansion. (**B–D**) E13 SMG were isolated and treated with anti-NRTN function blocking antibody for 24 h before being fixed and immunostained for nerves (**C**, Tubb3, green) and ZO1(+) tight junctions (**D**, white). Arrowheads highlight

ZO1 at the ductal midline. Scale bars: **C** = 50 μm; **D** = 20 μm. **C** is a 30 μm projection of 1.5 μm confocal sections. **D** is a 12 μm projection of 1 μm confocal sections.
See also Figure S1.

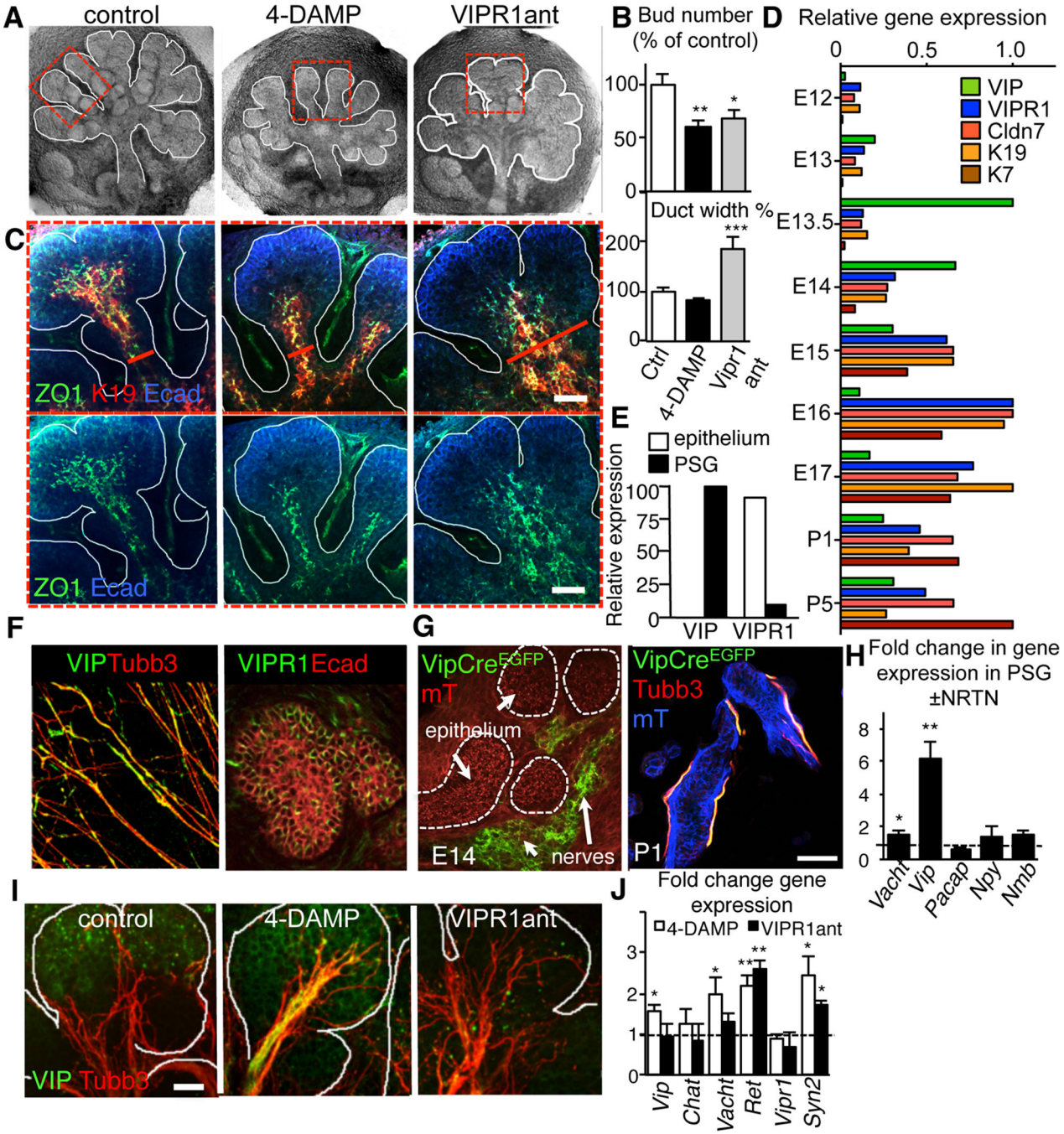

Figure 2. Ductal tubulogenesis requires VIP/VIPR1 but not ACh/M1 signaling

(**A–D**) E13 SMG were cultured with the muscarinic receptor antagonist, 4-DAMP (10 μM) or VIPR1 antagonist (VIPR1ant, 30 μM) for 24 h and, (**A**) overall architecture of the SMG; (**B**) branch number and duct width; (**C**) distribution of K19 (red) and ZO1 (green) with E-cadherin (Ecad, blue); (**D**) Microarray analysis of gene expression in SMG from embryonic day 12 – 17. Shown are relative expression levels (normalized to the highest expression level). **E)** SMG epithelial and mesenchymal compartments were separated and expression of VIP and VIPR1 were analyzed by qPCR. (**F**) E13 PSGs were isolated and immunostained

for neurons (Tubb3, red) and VIP (green) or E13.5 SMG were immunostained for E-cadherin (Ecad, red) and VIPR1 (green). (**G**) *Vip-Cre* mice were crossed to a *Rosa26*^{mTmG} reporter strain and the salivary glands analyzed at E14 and P1. Images represent 10–15 μm projections of 1 μm confocal sections. Scale bar = 50 μm. (**H**) E13 PSG were treated with 10ng/ml NRTN for 24h and changes in gene expression quantified by qPCR. (I and J) E13 SMG were cultured with the muscarinic receptor antagonist, 4-DAMP (10 μM) or VIPR1 antagonist (VIPR1ant, 30 μM) for 24 h and (**I**) neuronal outgrowth (Tubb3; red) and VIP protein (green) or (**E**) expression of neuronal marker transcripts were analyzed. In **E**, control expression was set to 1 (dashed line). Fluorescent images are 12 μm projections of 1 μm sections (in **C**) or 25 μm projection of 1.5 μm sections (in **D**). Scale bars: C = 50 μm; D = 20 μm. In **B** and **E**, data are means ± s.d. for 3 experiments. In **B**, data were analyzed using a one-way analysis of variance with post hoc Dunnett's test; in **E**, a false discovery rate (Q) for multiple unpaired t-tests was set to 5%; *P<0.05; **P<0.01; ***P<0.001.
See also Figure S2.

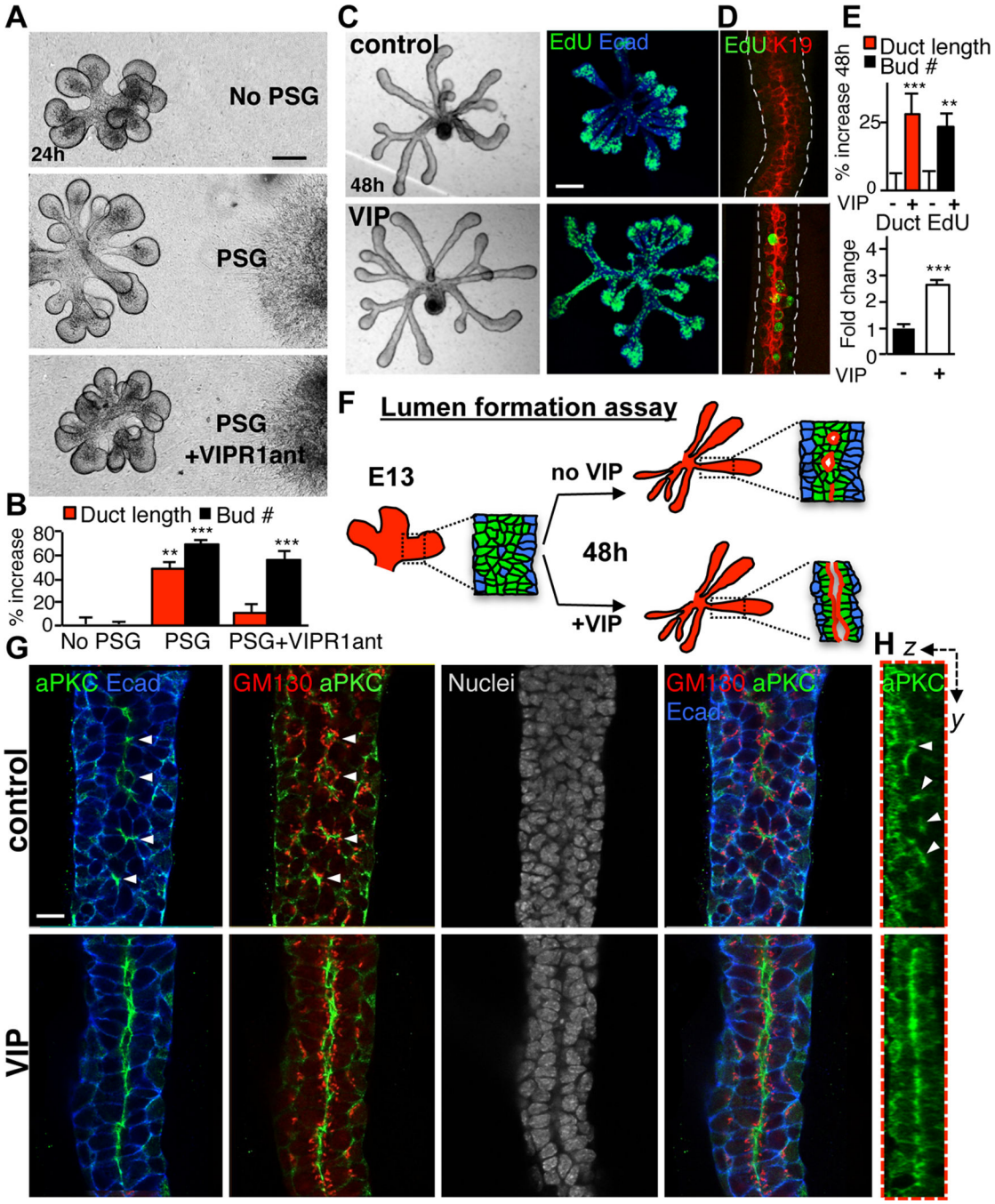

Figure 3. PSG-derived VIP promotes ductal growth and formation of a contiguous lumen

(**A** and **B**) E13 epithelia were co-cultured with isolated PSGs for 24 h ±VIPR1ant (30 μM). Representative images are shown in **A**; duct length and branch number were measured and quantified in **B**. Scale bar = 100 μm. (**C–E**) VIP promotes proliferation of ductal cells, ductal elongation and branching. Epithelia were cultured ±VIP (200 nM) for 48 h. The majority of EdU(+) with VIP treatment were luminal K19(+) cells (**D**). EdU-positive cells were counted and normalized to ductal area (**E**, lower graph). Fluorescent image is a 60 μm projection of 4 μm confocal sections. Scale bar = 100 μm. (**F**) Schematic illustration of the

lumen formation assay and observed experimental outcomes shown in **G**. (**G**) Apical-basal polarity was analyzed by immunolabeling for aPKC, apical membrane marker; E-cadherin, basolateral membrane marker; GM130, Golgi marker and Dapi, nuclei. Single 1.5 μm sections. Scale bar = 10 μm. (**H**) Z-sections along Y-axis. Arrowheads point to microlumens. Image is a 30 μm projection of 0.4 μm confocal sections. In (**B** and **E**), data are means ± s.d. of 3 experiments. In **B**, data was analyzed using a one-way analysis of variance with post hoc Dunnett's test. In **E**, a Students t-test was performed; ***P<0.001, **P<0.01, *P<0.05. See also Figure S3.

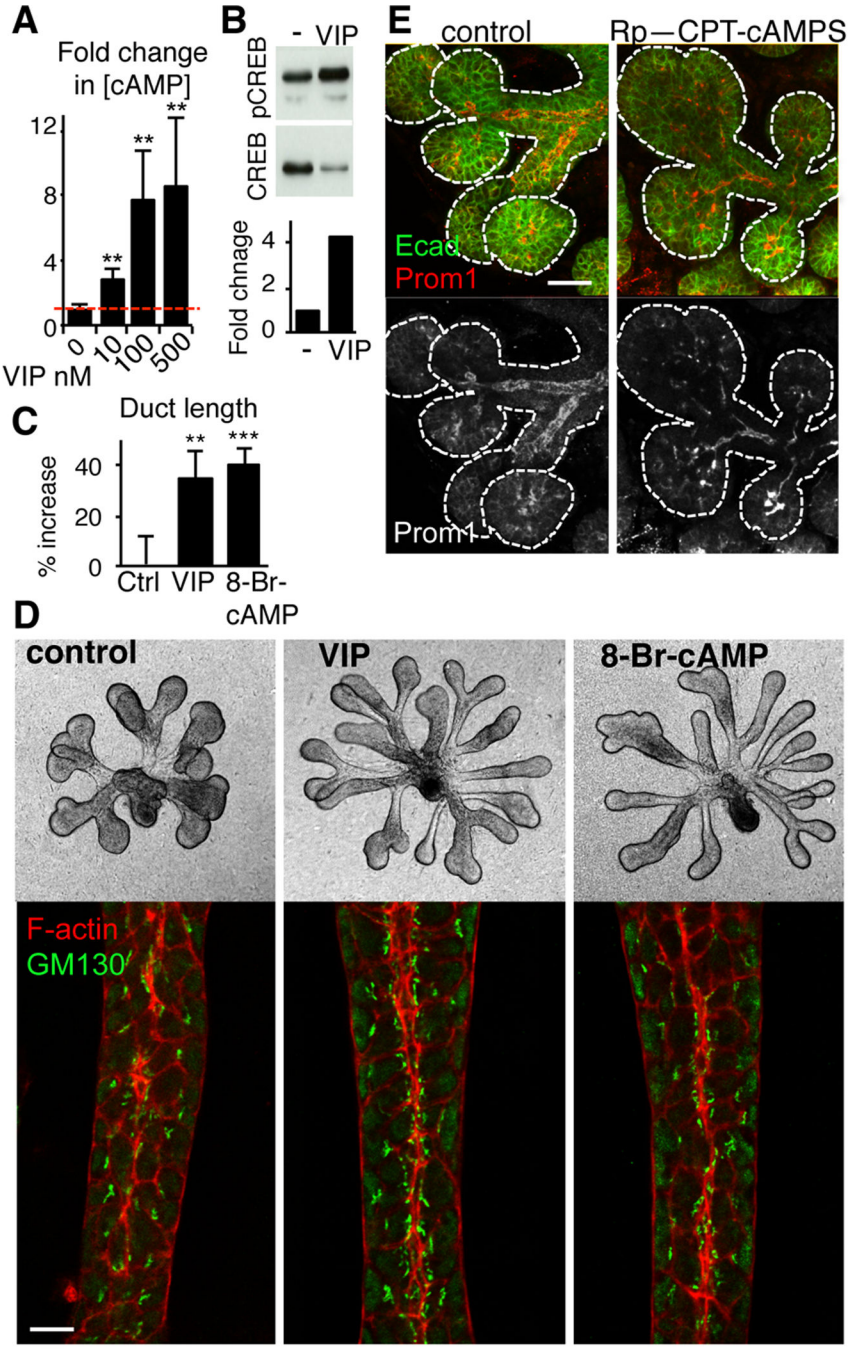

Figure 4. VIP mediates duct growth and lumen formation via a cAMP/PKA pathway

(**A** and **B**) VIP (concentrations indicated in A; 200 nM in B) increases cAMP (**A**) and CREB phosphorylation (**B**) levels in epithelial rudiments. (**C** and **D**) cAMP analog, 8-Br-cAMP, mimics the effect of VIP on ductal growth and formation of a contiguous lumen in epithelial rudiments. GM130 (Golgi, green) and F-actin (red) demarcate the luminal surface along the ductal midline. Duct length was quantified in **C**. Data are means ± s.d. of 3 experiments and were analyzed using a one-way analysis of variance with post hoc Dunnett's test; **P<0.01, ***P<0.001. Scale bar = 10 μm. (**E**) Inhibition of PKA results in aberrant lumen formation.

Intact E14 salivary gland was treated with 50 μM Rp-CPT-cAMPS (PKA inhibitor) for 24 h. Prominin-1 (prom1, green), luminal membrane marker, was used to highlight developing lumens. E-cadherin (Ecad, in blue) marks epithelial cells. Scale bar = 25 μm.
See also Figure S4.

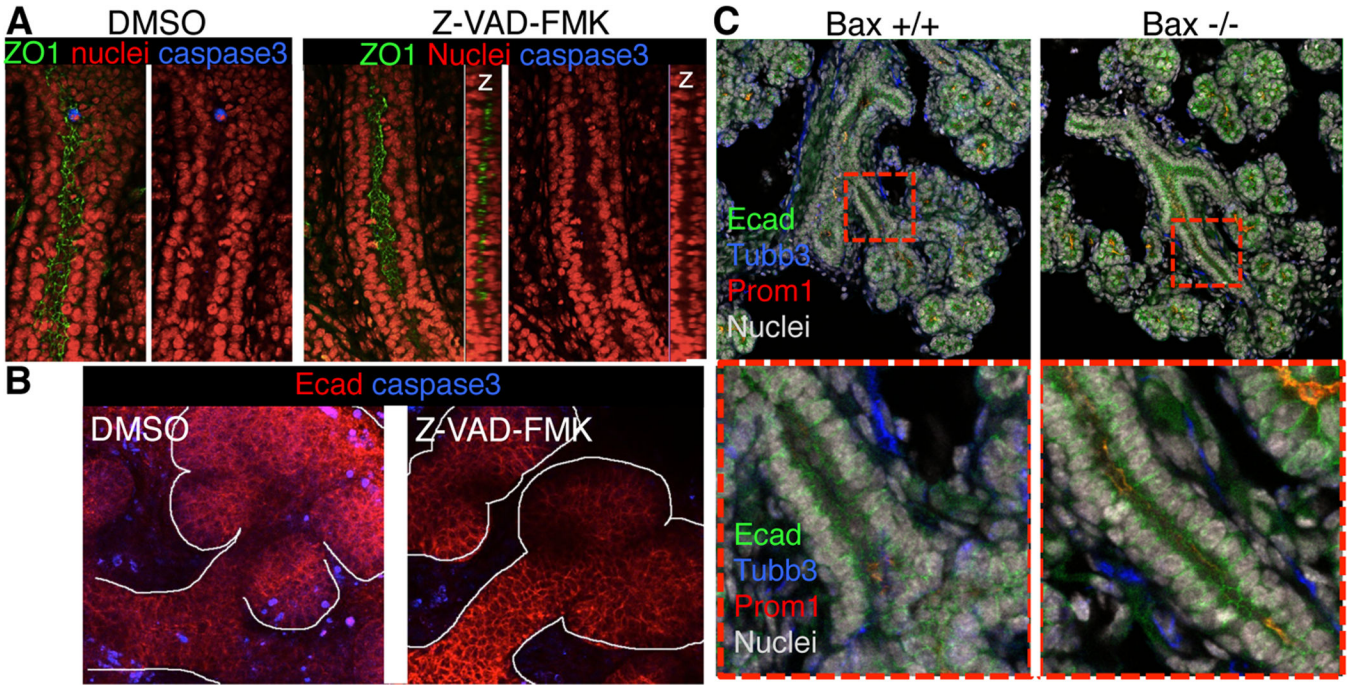

Figure 5. Inhibition of apoptosis does not prevent lumen formation in SMG

(**A** and **B**) E13.5 SMGs were cultured for 24 h in the presence or absence of the pan-caspase inhibitor Z-VAD-FMK (50 μM) before being fixed and immunostained for ZO1 and cleaved caspase-3. Images in **A** are 2 μm sections and in **B** are 70 μm projections of 3 μm confocal sections to show reduction of apoptotic cleaved caspase-3-positive cells in the mesenchyme of the DMSO- but not in Z-VAD-FMK-treated SMGs. **C**, E17 SMG from wild type (*Bax* +/+) and Bax deficient (*Bax* −/−) were fixed and stained for Ecadherin (green), Prominin-1 (red), nerves (Tubb3, blue) and nuclei (grey). Images are 2μm confocal sections.

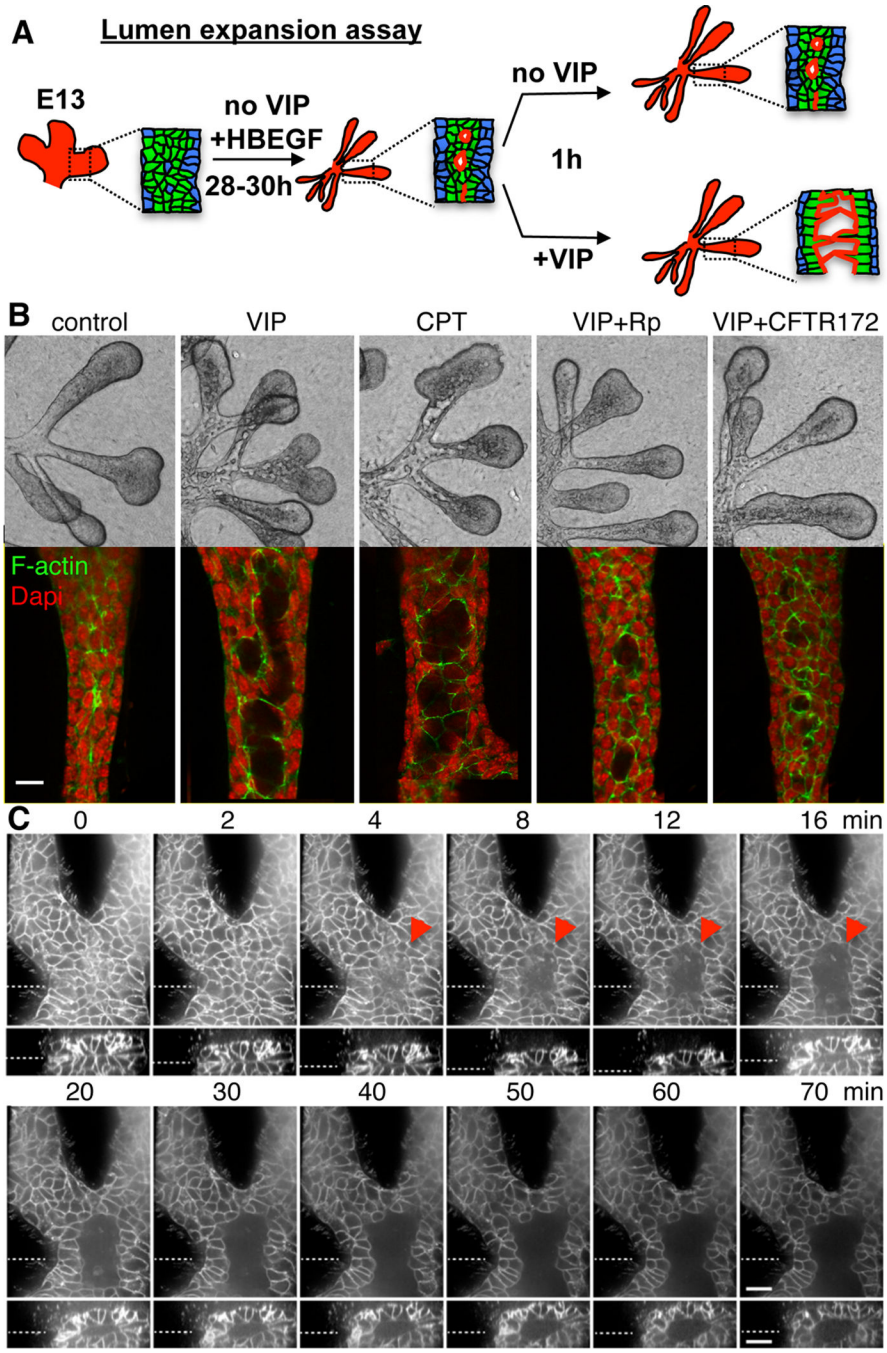

Figure 6. VIP regulates lumen expansion in a cAMP/PKA/CFTR-dependent manner

(**A**) Schematic showing lumen expansion assay and observed experimental outcomes. (**B**) E13.5 epithelia were treated with VIP, cAMP analog CPT-cAMP (CPT; 200 μM), PKA inhibitor Rp-CPT-cAMPS (Rp; 200 μM) or inhibitor of CFTR (CFTR-172, 40 μM) for 1 h. Fluorescent images are single 1μm confocal sections. Scale bar = 10 μm. (**C**) Epithelia with pre-formed ducts from mice expressing membrane-bound RFP (Tomato) were treated with VIP at time point 0 and lumen expansion was followed for 70 min. Top panels are single confocal XY-sections. The bottom panels are Z-axis reconstructions of 37 individual 1 μm-

spaced optical sections. Dashed lines indicate location of optical sections and Z-reconstructions. Arrowhead marks expanding lumen. Scale bars = 20 μm.
See also Figure S5.

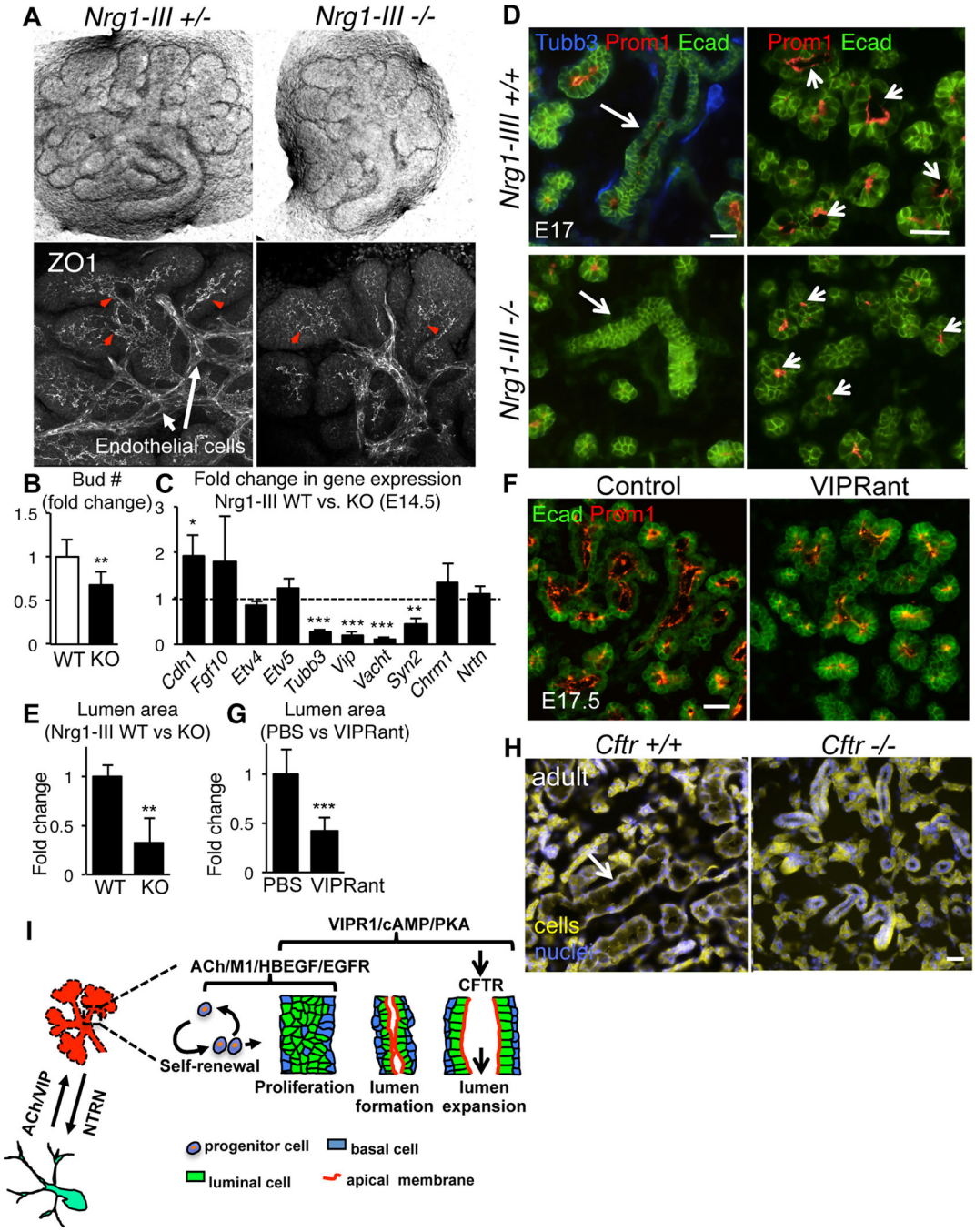

Figure 7. Depletion of VIP+ innervation *in vivo* abrogates epithelial branching, lumen formation and lumen expansion

(**A–D**) E14 salivary glands derived from *Nrg1-III*-null embryos cultured 24 h before buds were counted (**B**) and tissue was fixed and immunostained for ZO1 (grey). Images in **A**, lower panel, are 20 μm projections of 2 μm confocal sections. Arrowheads highlight ZO1 accumulation in presumptive ducts. (**C**) qPCR analysis of *Nrg1-III*-null E14 SMGs (control dotted line at 1). Means ± s.d. from 3 experiments. Data in **B** was analyzed by Students t-test. In **C** a false discovery rate (*Q*) for multiple unpaired t-tests was set to 5%; *P<0.05;

P<0.01; ***P<0.001. (D–E**) E17 SMG from wildtype and *Nrg1-III*-null mice. (**F–G**) Timed pregnant CD1 mice were injected 2× daily with VIPRant for 5 days; glands were analyzed at E17.5. In D–E and F–G, SMG E-cadherin (green) labels epithelium, Tubb3 (blue) neurons and Prominin-1 (Prom-1, red) lumens. **D** and **F** are epifluorescent images of 12 μm sections. Size of lumens in **D** and **F** was quantified by measuring the luminal area and normalizing to controls (expressed as a ratio; **E** and **G**). Data are means ± s.d. of 2 experiments (n=6, 3–4 glands per genotype/treatment) and were analyzed using the Student's **t**-test; **P<0.01; *<0.01. Scale bars = 50 μm. (**H**) Comparison of wild type and Cftr-deficient (S489×) salivary glands from 4 month female mice. Arrow highlights granulated duct. Glands were imaged using auto fluorescence (yellow) and nuclei were stained with Dapi (blue). (**I**) Schematic illustrating the role of ACh, VIP and NRTN in regulating SMG development.

See also Figure S6.